High-Throughput Characterization of Nanoscale Topography for Hybrid Bonding by Optical Interferometry

Bongsub Lee
Adeia Inc.
San Jose, CA, USA
Bongsub.Lee @adeia.com

Oliver Zhao
Adeia Inc.
San Jose, CA, USA
Oliver.Zhao@adeia.com

Arianna Avellán
Adeia Inc.
San Jose, CA, USA
Arianna.Avellan@adeia.com

Suhail Sadiq
Adeia Inc.
San Jose, CA, USA
Suhail.Sadiq@adeia.com

Gill Fountain
Adeia Inc.
San Jose, CA, USA
Gill.Fountain@adeia.com

Dominik Suwito
Adeia Inc.
San Jose, CA, USA
Dominik.Suwito@adeia.com

Guilian Gao
Adeia Inc.
San Jose, CA, USA
Guilian.Gao@adeia.com

Laura Mirkarimi
Adeia Inc.
San Jose, CA, USA
Laura.Mirkarimi@adeia.com

***Abstract*—Hybrid bonding requires nanoscale topography control of the surfaces to be bonded. Such topography is conventionally characterized by atomic force microscopy (AFM), which provides high accuracy but very limited throughput. In this study, we present a protocol to analyze the nanoscale metal recess and its wafer-level uniformity by phase shift interferometry (PSI) with a throughput three orders of magnitude greater than typical AFM analysis. Using an automated protocol, we analyzed ~ 10 million Cu pads and constructed a recess uniformity map for a full wafer. It confirmed that our CMP process could control the wafer-level recess variation within a few nm. While PSI has clear advantage in the data throughput, the limitations of PSI should also be considered. PSI has a limited lateral resolution of ~ 0.5 µm compared to its nanoscale z-resolution. The apparent Cu recess measured by PSI from Cu/SiO_2 samples is greater than the physical recess by an offset of tens of nm, based on the different phase change on reflection from different areas. This offset value varies with Cu surface oxidation or different thickness of transparent SiO_2. If SiO_2 is thicker than ~ 2 µm, the structures below the layer do not make significant impact. When the sample configuration and surface conditions are the same over the sample(s) to be analyzed, PSI can efficiently characterize the topography variation of numerous Cu pads on a die, a wafer, or multiple sets of wafers. This technique can be useful in controlling the process conditions to reduce the variation in critical topography parameters and improve hybrid bond yield.**

Keywords—hybrid bonding, nanoscale metrology, nanoscale topography, phase shift interferometry, atomic force microscopy

I. INTRODUCTION

Hybrid bonding, also called Direct Bond Interconnect (DBI®), forms a solder-free and organic-free interface between wafers or dies for 3D integrated circuits. It is a platform technology that enables sub-micron interconnect pitch, higher bandwidth, and greatly enhanced electrical/thermal performance compared to conventional solder-based thermal compression bonding or mass reflow [1] [2]. This technology is used for mass production of CMOS image sensors, 3D NAND memory, and 3D chiplet SoC for high performance computing [1] [3] [4]. Additionally, it is expected to be a key solution for the next-generation 3D integrated circuit applications in stacked DRAM [5] [6]. A requirement for successful hybrid bonding is nanometer-scale surface topography control of the wafer or die before bonding [7] [8]. The surface for hybrid bonding is a dielectric area (typically SiO_2) surrounding metal interconnects (typically Cu) for electrical connection, as illustrated in Fig. 1. Chemical mechanical polishing (CMP) must achieve a very low dielectric roughness and a desired recess of metal below the dielectric [7].

Efficient characterization of nanoscale topography is essential for process-metrology feedback in hybrid bonding assembly processes. Atomic force microscopy (AFM) is a very accurate topographic characterization method based on its sub-nm resolution in both vertical and lateral dimensions. We have reported methods and specific considerations for characterizing hybrid bond surfaces by AFM [8]. However, AFM has a low data acquisition rate (typically several minutes per image) and small imaging area (< 100 µm x 100 µm), which limits the statistical confidence for process development and metrology verification. For example, a wafer may have more than a

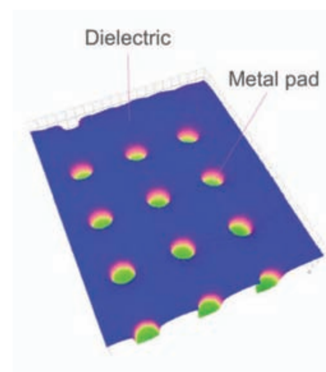

Fig. 1 3D representation of a surface for hybrid bonding, with dielectric background area and many metal pads.

2377-5726/24/$31.00 ©2024 IEEE
DOI 10.1109/ECTC51529.2024.00157

hundred million metal pads, and AFM can typically measure hundreds of pads in several hours even with an automated process. In contrast, advanced optical profilometry techniques can provide drastically higher throughput than AFM for statistical analysis. Phase shift interferometry (PSI), a commercially available technique with sub-nm vertical resolution, provides about three-orders of magnitude higher throughput based on its higher acquisition rate (seconds per image) and larger imaging size (300 µm - 4 mm) compared to AFM. PSI can often be confused with white light interferometry (WLI), since many commercial WLI systems also provide a PSI mode, but PSI utilizes monochromatic light and has better vertical resolution. Previously, the applicability of PSI for hybrid bonding has been introduced [9] [10], but not discussed in much detail.

While PSI provides clear advantages in data throughput and z height resolution, users should understand the limitations to avoid misinterpretation. First, conventional optical profilometry techniques including PSI have a lateral resolution of about 0.5 µm, which is not suitable to measure some parameters such as dielectric roughness due to the sub-nm lateral resolution requirement. The half-micron lateral resolution is sufficient to measure the metal pad size (microns) in almost all current hybrid bonding cases, while not good for sub-µm pitch. Secondly, the height data obtained by most high-resolution optical profilometry techniques including PSI depend on the refractive indices of the materials to be analyzed. If a surface has two areas of dissimilar materials, the techniques may indicate an inaccurate step height at the boundary. PSI is not to be confused with chromatic white light (CWL) profilometry, which is insensitive to refractive index but has a z-resolution of about 10 nm [11] that is insufficient for hybrid bonding. In the case of PSI, different amounts of phase change on reflection (PCOR) occur from different materials [12] [13] based on their refractive indices, which causes some inaccuracies with the actual recess. A hybrid bond surface has metal and dielectric areas, so the *apparent* metal recess shown by PSI is different from the *physical* recess that can be measured by AFM. Moreover, since the dielectric materials commonly used for hybrid bonding are transparent, the optical reflections from the surface and the interface(s) below the transparent bond surface can collectively contribute to the overall phase shift data.

In this study, we show a calibration process for Cu/SiO_2 hybrid bond samples by comparing the PSI and AFM data over a large range of recess or protrusion values. We provide examples of the change in PSI topography data based on variations of sample configuration (SiO_2 thickness and underlying interfaces) and surface state (Cu oxidation). When those conditions are the same over the samples to be analyzed, it is more straightforward to study the uniformity or repeatability of topography. Our automated protocol for PSI data acquisition and analysis allows easy analysis of hundreds of thousands of metal pads within hours. We present a wafer-level recess uniformity map, constructed by analyzing ~ 10 million Cu pads on a wafer without interruption. In addition, the statistical parameter variation in PSI data is evaluated as a method for process control feedback.

II. Experimental Procedures and Considerations

A. Hybrid Bonding Sample Preparation

We prepared multiple samples designed for hybrid bonding development to understand the versatility of this technique. The surface had SiO_2 background area with Cu pads as depicted in Fig. 1. Some samples had a 1.4 µm-thick BEOL (back end of the line) layer with SiO_2 and Cu pads (10 µm diameter and 40 µm pitch) on the top, with no redistribution layer (RDL) under it (Fig. 2(a)). Another sample had a 2 µm-thick BEOL layer on the top, with an underlying Cu redistribution layer (RDL) (Fig. 2(b)). We also used a 200 mm wafer, which consisted of a 3.5 µm-thick top BEOL layer, a 0.5 µm-thick via layer, and a Cu RDL layer (Fig. 2(c)). The top Cu bond pads had a 3.5 µm diameter with a 7 µm pitch [9]. We also characterized a wafer with defects such as pinholes in Cu pads or surface damage, to study the capability of PSI in finding defective areas.

We used our CMP processes and various sample preparation steps to prepare a wide range of recess or protrusion (negative recess) values to exercise the sample variation in this metrology development project. The surfaces were treated to intentionally control CuO_x on the Cu pad.

B. Metal Recess Analysis

Metal recess is defined as the depth of each metal pad below the dielectric surface level. From a hybrid bond surface such as Fig. 1, one can draw a line profile showing the metal and dielectric levels. Fig. 3(a) is a schematic example of such a profile. Real sample surfaces can have nonzero curvature or roughness, and the metal recess may be measured as the

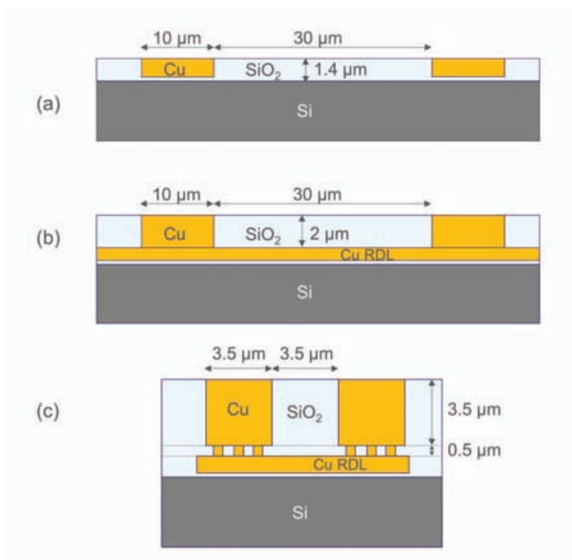

Fig. 2 Design of hybrid bonding samples used in this study. All surfaces contain Cu bond pads and SiO_2 dielectric. (a) Structure without a redistribution layer (RDL), where the Si surface is visible through 1.4 µm-thick transparent SiO_2. (b) Structure with a Cu RDL layer that is 2 µm below the surface. (c) Fine-pitch structure with a 3.5 µm-thick BEOL layer on the top and a 0.5 µm-thick via layer on an RDL layer.

difference in the average heights of the metal regions and nearby dielectric areas [8]. It is also possible to use available software to construct a histogram of the surface height, as depicted in Fig. 3(b). Such a histogram shows a bimodal distribution showing peaks at the dielectric level and the metal level. If the distinction is clear between the two peaks, it is easy for the analysis software to recognize all the metal areas and collect the topographic data within each metal pad.

C. Automated PSI Procedure

Before taking PSI measurements, an autofocus and auto tip-tilt routine was run. The autofocus procedure ensures that the sample surface is at the same distance from the lens for each image, i.e. the sample is sitting in the same fringe of the greatest contrast. We found that choosing a different fringe could result in a deviation of 10 nm or more in measuring a standard 100 nm step. As a result, the autofocus procedure is critical for reliable and consistent data acquisition. The auto tip-tilt routine keeps the width of the fringes consistent across the field of view for each image.

To analyze a large number of Cu pads, we developed an automated protocol for PSI data acquisition and analysis. This protocol took PSI data from numerous areas on the wafer, distinguished the Cu pad areas from the SiO_2 background based on the bimodal height histogram, numbered every Cu pad, and recorded the recess value of every pad (mean depth within a pad area) as well as several other statistical parameters such as the peak-to-valley height difference R_t and the level of the lowest point R_v within each Cu pad.

D. PSI Data Calibration by AFM

We employed AFM to obtain the physical Cu recess values and compared them with corresponding PSI data. We obtained the surface profiles (as illustrated in Fig. 3(a)) from both the AFM and PSI data taken from the same sample locations, to record and compare the recess values.

While both contact and tapping modes of AFM could be effectively used, we preferred using a contact mode for this study to minimize possible artifacts. We reported [8] that incorrect Cu recess may be measured especially when the tip-to-surface force is very weak, since the tip-surface interaction could be affected by electrostatic charging or soft contaminants. A soft-tapping or non-contact mode was more prone to such an effect, and a hard-tapping mode usually provided good balance between data quality and tip life for analyzing hybrid bonding surfaces. The contact mode is the least prone to such artifact but could reduce the sharpness of a tip after a short period of use, causing a worse lateral resolution. For this study, we replaced the tip frequently and, even if the tip could become somewhat blunt, the lateral resolution was still expected be sub-nm or nm and far more than sufficient for measuring the recess of Cu pads that are many microns wide.

III. Results and Discussions

A. Correlation of PSI and AFM Data for Cu/SiO_2 Hybrid Bonding Samples

When PSI was performed on Cu/SiO_2 hybrid bonding samples, the Cu pads appeared to be deeper in the PSI data than in the corresponding AFM data. This is due to the different phase change on reflection from the two different areas, as discussed earlier. Fig. 4 shows the relationship between the Cu recess values measured by PSI and AFM from many sets of Cu pad areas on samples with 1.4 µm-thick SiO_2 on plain Si (Fig. 2(a)). The PSI and AFM data showed a simple linear relationship with a slope of 1.0 and an offset of 46 nm. The data scatter within a few nm could be the result of possible formation of CuO_x on some pads after cleaning and before measurement, non-uniformity between different sample areas, and measurement errors in each technique.

To test the effect of CuO_x formation, we created a 6 - 10 nm layer of CuO_x on the Cu pads. The offset between the PSI and

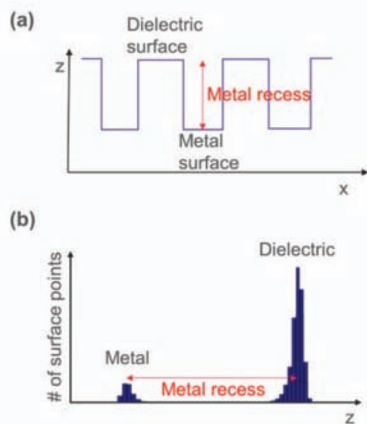

Fig. 3 (a) Schematic example of a topographic line profile from a hybrid bonding surface like Fig. 1, showing metal pad areas slightly recessed from the dielectric level. (b) Schematic histogram of the height values of all the surface points. If the peaks in this bimodal distribution are clearly separated, it is easy for an automated protocol to recognize each metal pad area from the topography data.

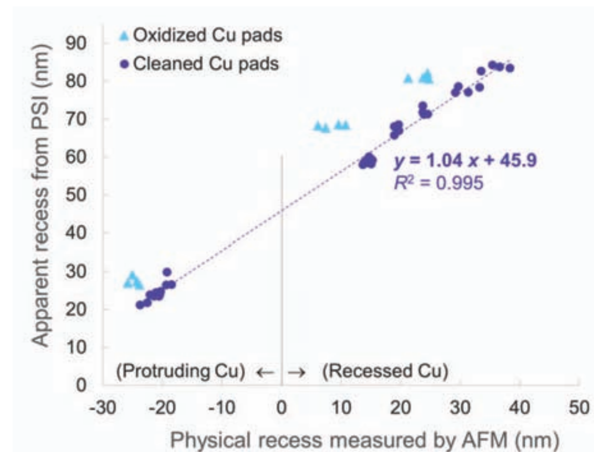

Fig. 4 Relationship between the *apparent* Cu recess measured by phase shift interferometry (PSI) and the *physical* recess measured by AFM, from a sample with 1.4 µm-thick SiO_2. There is an offset between PSI and AFM data due to the different phase change on reflection (PCOR) from the Cu and SiO_2 areas, which could be affected by Cu surface oxidation, SiO_2 thickness, and other factors.

AFM data became even greater by ~ 10 nm. In this case, AFM detects only the CuO_x surface on the pads, while PSI detects the combined optical responses from the CuO_x and Cu surfaces. This result suggests that problems like corrosion or contamination, damage, or porosity could also affect the PSI data, based on the apparent change in optical properties.

Different SiO_2 thickness could also affect the offset value. We tested a case with thicker SiO_2, with a wafer with a 3.5 µm-thick top BEOL layer and a 0.5 µm-thick via layer on buried Cu RDL (Fig. 2(c)). The offset between the PSI and AFM data was close to 35 nm, while we have not probed as many areas. The larger offset of 45 nm in the previous case should be the result of thinner SiO_2 and the underlying Si surface.

When the top transparent layer is sufficiently thick, the PSI data were insensitive to the underlying interfaces. From wafers with the aforementioned configuration with thick SiO_2 layers (4 µm in total) and Cu RDL, the buried RDL was visible under an optical microscope (Fig. 5(a)) but invisible in the PSI data (Fig. 5(b)), showing the negligible effect of the RDL on the PSI data. However, in a case with a ~ 2 µm SiO_2 layer on buried Cu RDL (Fig. 2(b)), the RDL pattern was visible on not only the optical micrograph (Fig. 5(c)) but also the PSI image (Fig. 5(d) with enhanced contrast). AFM did not detect the RDL pattern, which confirms that the pattern on the PSI image did not represent the actual surface topography but was the effect of the optical reflection from the buried Cu. This effect created an artifact, a step of ~ 1 nm or smaller in the PSI data, which was still very minor compared to the recess offset.

B. *Wafer-Level Uniformity of Metal Recess: Studying Millions of Pads*

The slope of the PSI-AFM correlation function was shown to be unity in the previous section, so one should know just the offset value in a given condition to measure metal recess by PSI. Moreover, even without obtaining the exact offset value, it is possible to study the relative *variation* of recess, as long as the stacking structure and surface conditions are reasonably the same across the samples. One can examine the recess uniformity across a die, a wafer, or many wafers.

We conducted a wafer-level recess uniformity study on a 200 mm hybrid bonding wafer with 7 µm Cu pad pitch with thick SiO_2, a design described before. Using an automated protocol we developed, we scanned the wafer (Fig. 6(a)) and took 22,610 PSI images (like Fig. 6(b)) over the wafer. Each PSI image included more than 420 Cu pads, e.g., 437 pads in Fig. 6(b). Therefore, we analyzed total of ~ 10 million Cu pads on the wafer, which is ~ 3 % of the total pads. Each Cu pad area was automatically separated from the surrounding SiO_2 area using the height histogram, and the recess of each Cu pad was recorded. Since the Cu recess measured by PSI is greater than the real recess, the apparent contrast between SiO_2 and Cu areas is more pronounced in a PSI image than in the corresponding AFM image for any recessed pads. This fact makes it easier for the software to automatically detect each Cu pad area. Our previous publication [9] employed this process and showed a plot of recess variation vs. radius.

Using the xy-coordinate corresponding to each PSI image and the average Cu recess value within each of them, we

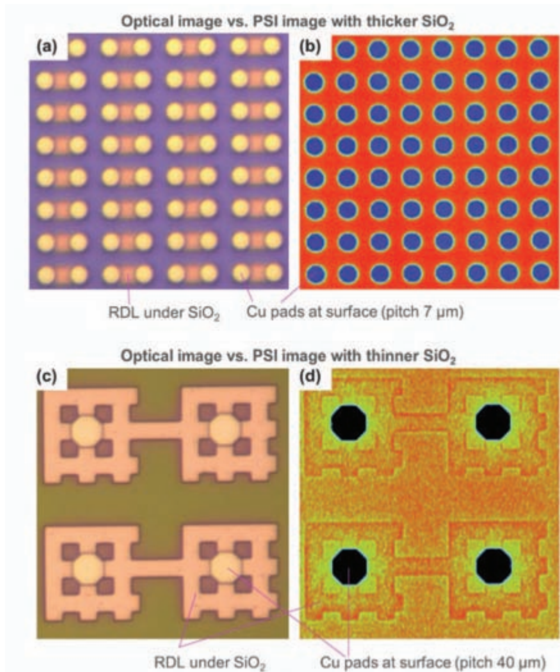

Fig. 5 Comparison of optical and PSI images from samples with different SiO_2 thickness. (a) Optical micrograph of a sample with relatively thick SiO_2 (4 µm) and (b) PSI image from an equivalent sample, which does not show the Cu RDL areas buried under the transparent SiO_2. (c) Optical micrograph of a sample with thinner SiO_2 (~ 2 µm)) and (d) PSI image from an equivalent sample, which shows the RDL areas (with enhanced contrast). This suggests that, if a transparent layer is sufficiently thick, the structure under the layer has insignificant effect on the PSI topography data.

constructed a recess variation map of the wafer, which is shown in Fig. 6(c). Metal pads on this wafer were populated on an array of rectangular die areas and not on the test areas between those rectangles. Hence, the recess variation data were shown only on those areas populated with Cu pads. This map clearly shows radial symmetry of the recess resulting from our CMP process. The Cu recess was slightly smaller (shallower) near the center and the very edge, while slightly larger (deeper) near the mid-radius of this wafer. The range of variation was within only a few nanometers from the mean recess, based on the well-controlled CMP process. It was not practical to use AFM to construct such a detailed recess map. We used AFM and analyzed metal recess on multiple wafers with respect to radius [14], but far fewer sets of data were available due to the limited throughput of AFM.

This method with PSI can be advantageous in a high volume production setting, where a large number of wafers or dies must be sampled. PSI could easily produce about three-orders of magnitude more data than AFM within the same time due to the greatly higher imaging speed and larger imaging size. Nonuniformity in PSI data may represent recess variation as well as possibly dissimilar surface conditions or layer thickness. When necessary, AFM can still be used to sample a small number of areas to confirm the actual topography since AFM

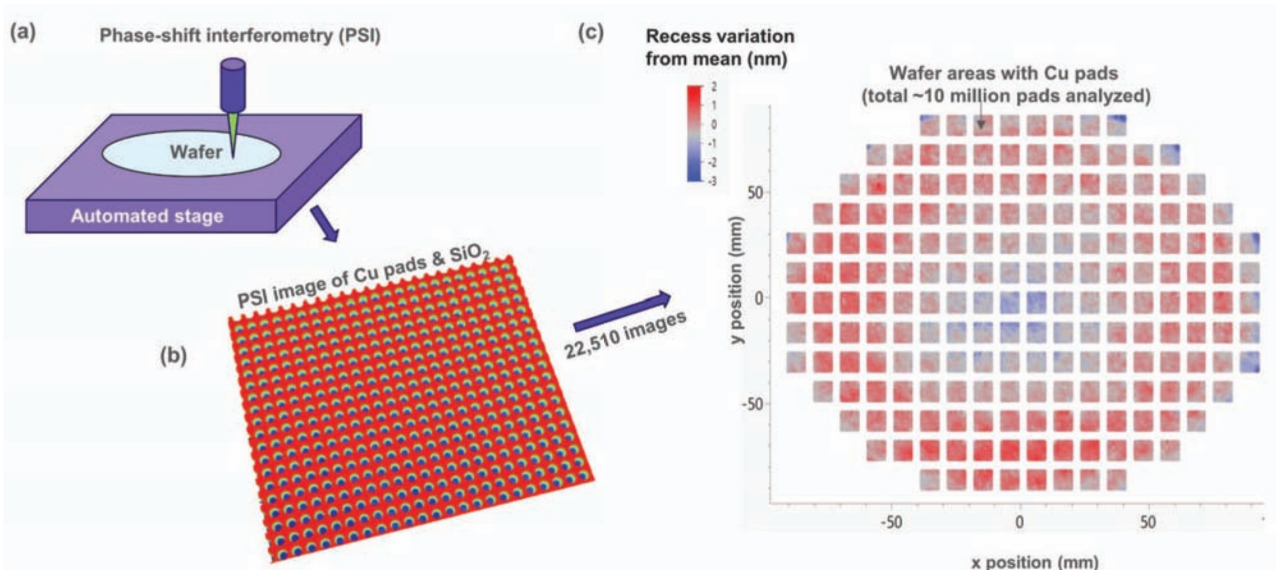

Fig. 6 Wafer-level Cu recess variation analyzed by (a) performing phase shift interferometry on many locations of a wafer, (b) obtaining the recess of each pad in the PSI images, and (c) constructing a wafer-level map using the data from ~ 10 million total Cu pads in 22,510 PSI images. Each data point in this map shows the average Cu recess within a PSI image covering about 160 µm x 140 µm. The CMP process tightly controlled the wafer-level recess variation within a few nm. This map also reveals the radial symmetry resulting from the CMP steps.

provides high accuracy and is not affected by the combined optical responses from the sample structure. Depending on the setting, AFM may be performed on one wafer per lot or when there is unexpected nonuniformity or scatter in PSI data for verification.

C. *Defect Characterization by Examining Statistical Parameters*

Statistical evaluation of PSI data can be helpful in locating certain kinds of defects, such as damaged or irregular metal structures. It is possible to program the software to collect multiple statistical parameters from the topography of each metal pad. The previous section discussed the recess value of each pad (mean depth of the surface within a pad area). The recess map showed the average recess of more than 420 pads in each PSI image, but it is certainly possible to examine all the ~ 10 million individual recess values and find abnormal values. In addition, it is possible to utilize various other parameters such as R_v (the height level of the deepest point within one metal pad area), R_t (the peak-to-valley difference within a pad area), or the area of each metal pad, depending on the purpose of analysis.

For example, we could use R_v to find defective metal pads. If all metal pads included in a PSI image have relatively flat surfaces as depicted in Fig. 7(a), each of the pads should show a similar R_v value, so the standard deviation of R_v within the PSI image should be close to zero. However, if one metal pad has a deep pit as in Fig. 7(b), the R_v from the pad area is very different from the normal pads, and therefore the standard deviation of R_v within this PSI image is large. We used a wafer with some metal damages and took more than 3500 PSI images using an automated protocol. The recipe obtained the standard deviation of R_v from each of the PSI images, and all of them are plotted in Fig. 8(a). Most images show small standard deviations in R_v, but several of them show distinctively high values. Each of those exceptional locations contained certain defects. Figs. 8(b), (d), and (e) include small holes or scratches in some Cu pads. Fig. 8(c) has an area of missing pads and irregular pads. R_t may be used in a similar manner.

This method is obviously very effective in finding such small defects, which are not always easy for a human inspector to locate from PSI or optical images. Performing a general inspection is still important to analyze other kinds of defects including metal discoloration, foreign materials on dielectric, and various patterning defects. To help this process, we conducted an advanced study to implement machine learning to automatically analyze and categorize numerous optical micrographs, discussed in a separate report [15].

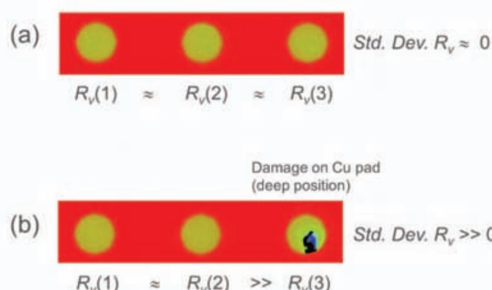

Fig. 7 Illustration of the usage of R_v (level of the deepest point in a Cu pad). (a) Example PSI image with flat Cu pads, all with similar R_v values. (b) PSI image with a damaged metal pad, hence with a very low R_v. The standard deviation of R_v obtained from this image is much greater than zero. Therefore, a large standard deviation in R_v is an indicator of defects.

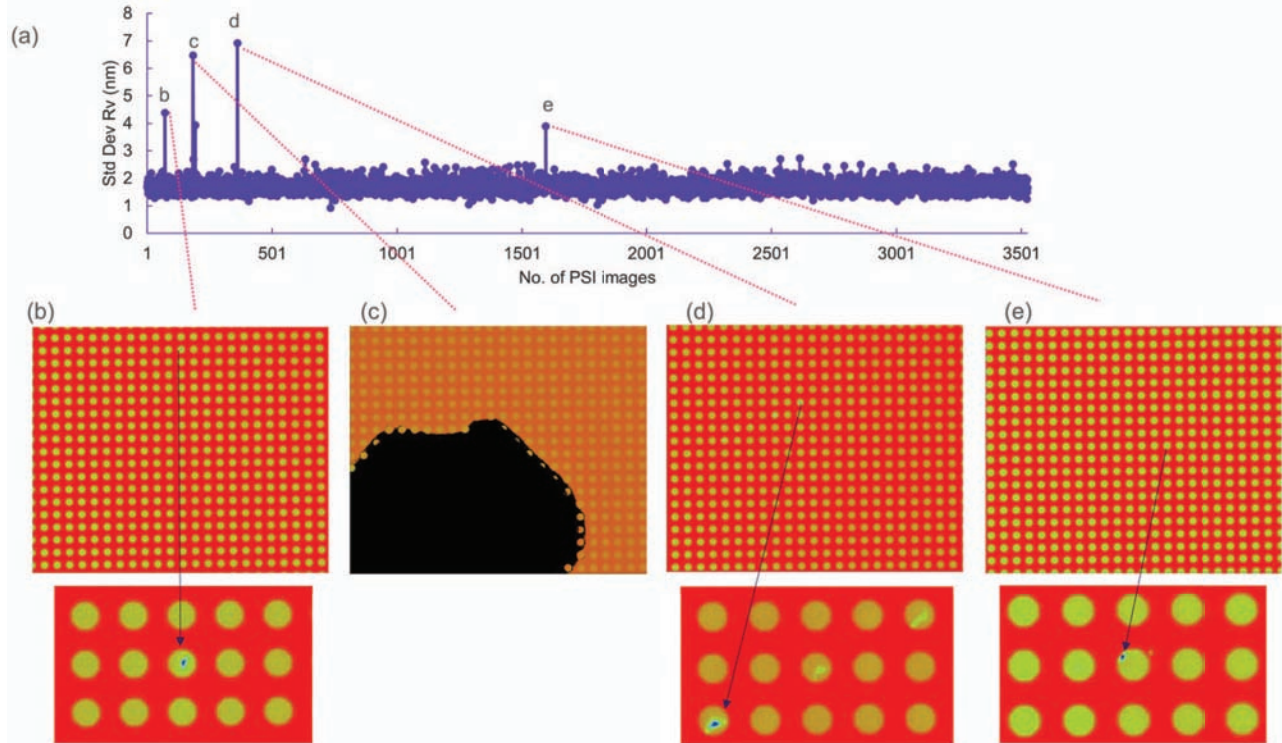

Fig. 8 Example of defect characterization based on surface topography parameter R_v. (a) Collection of the standard deviation of R_v from ~ 3500 PSI images. (b)-(e) Images corresponding to the positions with abnormally high standard deviation of R_v. The abnormal values indicate defects such as pits, scratches, or missing pads. Compared to manually examining all ~ 3500 images, this procedure provides an effective way to locate such defects.

IV. Conclusions

We employed phase change interferometry (PSI), an advanced optical profiling technique, to characterize the nanoscale topography of Cu/SiO_2 samples prepared for hybrid bonding. This technique provided about three orders of magnitude higher throughput compared to AFM, which made it practical to conduct statistical analysis of 10^5 - 10^7 Cu pads. Using an automated protocol, we could monitor the metal recess uniformity on a full wafer or multiple different samples. In addition, evaluation of surface parameters from many sets of PSI data was efficient in locating certain kinds of sample defects, such as damaged or irregular metal structures.

Since PSI data are affected by the different optical responses from the metal and dielectric areas of a hybrid bonding sample, we conducted a comparative study of PSI and AFM data with respect to various Cu recess or protrusion values. For a sample with 1.4 µm SiO_2 on Si, the PSI and AFM data showed a linear relationship with a slope of 1.0 and an offset of 46 nm. The offset value became apparently higher if the Cu surface was oxidized. The offset could also vary with the SiO_2 thickness, being around 35 nm from a sample with much thicker SiO_2. The metal structure buried under transparent SiO_2 could also affect the PSI topography data, but it was minimal if the top SiO_2 layer was ~ 2 µm or thicker. As exemplified by these results, it is important to understand that the PSI data depend on the sample structure (surface materials, transparent layer thickness, and materials under the transparent layer) as well as the surface condition (oxidation, corrosion, porosity, or contamination). In addition, it should be noted that PSI is applicable to features that are sufficiently larger than the lateral resolution limit of ~ 0.5 µm.

When the structure and surface conditions are uniform over the sample(s) to be analyzed, PSI could easily be utilized to characterize the topography of numerous metal pads. The data may be calibrated by AFM on a small number of areas if necessary, for example, on one wafer per lot or when unexpected nonuniformity is observed. Our wafer-level uniformity study based on this technique could reveal any process-related trends such as radial symmetry of Cu recess resulting from the CMP steps and tight control of recess variation within a few nm. Therefore, this methodology can be used to control the process conditions to reduce the variation in topography for hybrid bond yield improvement.

Acknowledgment

The authors thank Marjorie Cara, Marita Adsuara, Geraldo Ayala, and Pawel Mrozek for their help on sample and data processing.

REFERENCES

[1] L. Mirkarimi, "3D chiplet integration with hybrid bonding," Chip Scale Review, pp. 7-11, 2023.

[2] G. Gao and L. Mirkarimi, "Chapter 3: Hybrid Bonding Process Technology," in Direct Copper Interconnection for Advanced Semiconductor Technology, D. Shangguan, Ed. CRC Press, in press.

[3] Kagawa, Y., Noriko Fujii, K. Aoyagi, Yusaku Kobayashi, Susumu Nishi, N. Todaka, S. Takeshita, Joseph Charles Taura, H. Takahashi, Y. Nishimura, Keiji Tatani, M. Kawamura, H. Nakayama, Takashi Nagano, K. Ohno, Hayato Iwamoto, S. Kadomura and Teruo Hirayama, "Novel stacked CMOS image sensor with advanced Cu2Cu hybrid bonding," 2016 IEEE International Electron Devices Meeting (IEDM), 2016.

[4] P. Clark, "China's YMTC takes lead i n 3D-NAND memory," EETimes, Technology News, April 13, 2020.

[5] J. Park, B. Lee, H. Lee, D. Lim, J. Kang, C. Cho, M. Na and I. Jin, "Wafer to Wafer Hybrid Bonding for DRAM Applications," Proc. IEEE 72nd Electronic Components and Technology Conference (ECTC), San Diego, CA, USA, 2022.

[6] T.-H. Hung, J. Y.-J. Lo, T.-Y. Kuo, S.-Y. Shih, S.-F. Huang, Y.-L. Lin, H.-Y. Chiu, W.-Z. Li, H.-W. Hu, H.-H. Chang, C.-L. Shih, J. J. P. Lin and K.-N. Chen, "TSV Integration With Chip Level TSV-to-Pad Cu/SiO_2 Hybrid Bonding for DRAM Multiple Layer Stacking," IEEE Electron Device Letters, vol. 44, no. 7, pp. 1176-1179, 2023.

[7] P. Enquist, "3D Technology Platform – Advanced Direct Bond Technology," in 3D Integration for VLSI Systems, Pan Stanford Publishing, p. 175, 2011.

[8] B. Lee, P. Mrozek, G. Fountain, J. Posthill, J. Theil, G. Gao, R. Katkar and L. Mirkarimi, "Nanoscale topography characterization for direct bond interconnect," Proc. IEEE 69th Electronic Components and Technology Conference (ECTC), Las Vegas, NV, USA, 2019.

[9] L. Mirkarimi, T. Workman, J. Theil, G. Fountain, K. Bang, O. Zhao, B. Lee, C. Uzoh, D. Suwito and G. Gao, "Fine Pitch Die-to-Wafer Hybrid Bonding," in IEEE 73rd Electronic Components and Technology Conference (ECTC), Orlando, FL, USA, 2023.

[10] H. K. Niazi, B. Zhang, X. F. Brun, S. Krishnan and J. Chuang, "Critical Dimension Scatterometry as a Scalable Solution for Hybrid Bonding Pad Recess Metrology," in IEEE 73rd Electronic Components and Technology Conference (ECTC), Orlando, FL, USA, 2023.

[11] V. Siderov, D. Mladenova, R. Yordanov, V. Milenkov, M. Ohlidal, O. Salyk, I. Zhivkov and M. Weiter, "Film thickness measurement by optical profilometer MicroProf® FRT," Bulgarian Chemical Communications, vol. 45, no. Special Issue B, pp. 194-197, 2013.

[12] J. F. Biegen, "Determination of the phase change on reflection from two-beam interference," Optics Letters, vol. 19, no. 21, pp. 1690-1692, 1994.

[13] M.-C. Park and S.-W. Kim, "Compensation of phase change on reflection in white-light," Optics Letters, vol. 26, no. 7, p. 420, 2001.

[14] G. Gao, T. Workman, C. Uzoh, K. M. Bang, L. Mirkarimi, J. Theil, D. Suwito, R. Katkar, G. Fountain, G. Guevara and B. Lee, "Die to wafer stacking with low temperature hybrid bonding," in Proc. IEEE 70th Electronic Components and Technology Conference (ECTC), Orlando, FL, USA, 2020.

[15] O. Zhao, D. Suwito, B. Lee, T. Workman and L. Mirkarimi, "Deep convolution neural networks for automatic detection of defects which impact hybrid bonding yield," in press, in Proc. IEEE 74th Electronic Components and Technology Conference (ECTC), Denver, CO, USA, 2024.